PHILOSOPHICAL MAGAZINE A, 1996, VOL. 73, NO. 5, 1363–1383

On the contribution of screw dislocations to internal stress fields associated with dislocation cell structures

By D. RAABE

Institut für Metallkunde und Metallphysik, Kopernikusstr. 14, Rheinisch-Westfälische Technische Hochschule Aachen, 52056 Aachen, Germany

[*Received 22 August 1995 and accepted in revised form 24 October 1995*]

ABSTRACT

The internal elastic stress fields associated with dislocation cells are studied using numerical three-dimensional simulations. The paper deals exclusively with static dislocation arrangements. The dislocations are treated as line defects embedded in an otherwise linear isotropic elastic medium. The dislocation lines are decomposed into piecewise straight segments. Two types of three-dimensional dislocation ensemble are investigated. The first arrangement represents a conventional subgrain structure. It consists of pure small angle tilt and twist boundaries with alternating sense of misorientation according to the model of Kuhlmann-Wilsdorf. The second one consists of interface dislocations according to the model of Mughrabi. The stress fields of both types of cell structures are calculated both with and without screw dislocations. The simulations substantiate that in the first case (Kuhlmann-Wilsdorf) the contribution arising from screw dislocations is negligible. However, in the second case (Mughrabi) the screw dislocations lead to an increase in the maximum shearing stress in the cell interor by about 67%. The total value of the maximum shearing stress arising from screw and edge dislocations, τ^{3D}, can in the present case empirically be described by the expression $\tau^{3D} = \tau^{2D} + \tau^{2D}(1 - \nu)$ where τ^{2D} represents the contribution of the edge dislocations and $\tau^{2D}(1 - \nu)$ the contribution of the screw dislocations. The influence of the number of involved slip systems and of the boundary conditions on the internal stress fields are investigated. The latter results show that the stress fields of three-dimensional dislocation arrangements must be calculated for cells which are embedded in larger translational three-dimensional grids, in order to provide sufficiently accurate boundary conditions.

§ 1. INTRODUCTION

The numerical modelling of three-dimensional (3D) internal stress fields which are generated by crystal dislocations in metals is a pertinent tool required in formulating advanced flow stress theory. Together with the kinetic parameters of plastic deformation and additional external and internal stress sources arising from the presence of lattice defects other than dislocations, the internal stress fields enter the kinetic law of crystal plasticity. This kinetic part of the constitutive laws of crystal plasticity represents a mechanic equation of state, i.e. its result is determined by state variables rather than path dependent variables. When state variables are used to incorporate dislocation properties, they should not only reflect their global density but additionally their arrangement. For rough approximations the Taylor relation, which predicts that the stress is proportional to the square root of the dislocation density, is valid in many cases. However, its general application can nonetheless lead to inaccurate stress predictions if the dislocation arrangements

are neglected. Especially in the latter context, numerical 3D calculations of dislocation stress fields thus represent a helpful diagnostic means of testing, complementing and improving analytical approaches to the kinetic law of crystal plasticity.

In addition to these applications in the field of dislocation statics the internal stresses enter the calculation of the evolution of the dislocation structure during plastic deformation. This subject falls into the domain of dislocation dynamics. It represents an essential ingredient in formulating the structural evolution law. In contrast to the kinetic framework of crystal plasticity the structural evolution law depends on the microstructural path.

Crystal dislocations give rise to the generation of complex 3D stress fields. Furthermore, they arrange themselves in intricate 3D networks, which complicates the analytical treatment. Depending on the structural and kinetic parameters of deformation such dislocation arrangements often consist of dislocation cell walls with a high dislocation density and cell interiors with a low dislocation density. In two dimensions the calculation of internal stress fields which are associated with cell structures are typically confined to the consideration of edge dislocations. In two dimensions such simplification is admissible since it is the edge dislocations which mainly promote structure formation due to their anisotropic stress field (static argument) and limited mobility (dynamic argument). However in three dimensions, screw dislocations must additionally be considered. As was pointed out by Mughrabi, Ungár, Kienle and Wilkens (1986) in a note added in proof, the screw dislocations can generate similar internal stresses as edge dislocation. Neglecting them can thus lead to an under- or overestimation of internal stress fields. Hence, it is evident that 3D simulations, which principally include screw dislocations, allow a more realistic treatment of intricate dislocation arrangements as compared to two-dimensional (2D) approaches.

In the past considerable success was achieved in describing the statics of dislocation cells by the use of analytical methods. Among the various static approaches which served as ingredients in formulating the kinetic equation of state, the composite model (Mughrabi 1979) in particular, enriched by the introduction of interface dislocations (Mughrabi 1983) and the concept of low energy dislocation structures (Kuhlmann-Wilsdorf 1968) have stimulated progress in this field.

The predictions derived from both approaches depend on the correct description of the stress fields generated by the underlying type of cell structure. However, for complex 3D dislocation cell structures analytical calculations of internal stress fields are too complicated. Therefore, this paper concentrates on the numerical simulation of internal stresses associated with 3D cell structures. The geometrical complexity of such dislocation arrays, the large number of dislocations involved and the requirement for 3D approaches nowadays advocate the employment of numerical methods in this field. Encouraged by the rapid enhancement of computer facilities, numerical approaches are now increasingly being developed which allow the discrete description of single dislocations in both time and space (Kubin *et al.* 1992, Kubin 1993, Devincre and Condat 1992). This study concentrates on the numerical calculation of stress fields arising from two types of idealized 3D dislocation arrangements with special regard to the contribution of the screw dislocations. On the basis of these results the validity of corresponding 2D analytical and 2D numerical models is discussed.

Following the concept of Bassim, Kuhlmann-Wilsdorf and van der Merwe (Kuhlmann-Wilsdorf 1968, Bassim and Kuhlmann-Wilsdorf 1973, Kuhlman-

Wilsdorf and van der Merwe 1982) the first type of cell structure consists of small angle tilt and twist boundaries with an alternating sense of misorientation from one cell to the next. Such a dislocation arrangement is typically referred to as a subgrain structure. Following the model of Mughrabi (1983) the second cell structure consists of thick cell walls with a high content of dipoles which are enriched by so-called interface dislocations and cell interiors with a negligible dislocation content. Both dislocation cell types are among the elementary structure units of many observed dislocation arrangements.

§ 2. Simulation method

The analytical description of piecewise straight dislocations in three dimensions was pioneered by Yoffe (1960) and Hokanson (1963). They showed that for calculating the stress fields of simple dislocation arrays the dislocation lines may be decomposed into isolated segments. However, their approaches neglected the fact that dislocation segments should not generally terminate within an otherwise perfect region of crystal. Furthermore, in arbitrary dislocation arrangements consisting of straight dislocation segments, stress equilibrium was not maintained locally. As was discussed by Li (1965) and described in greater detail by DeWit (1965, 1967), a consistent tensorial 3D approach to the calculation of stress fields associated with piecewise straight dislocation lines is attained when the Burgers vectors are conserved at the dislocation nodes. Thus, for an adequate mathematical treatment line segments which are not integrated into the network must be semi-infinite or terminate at a free surface, a grain boundary or some other defect, where stress equilibrium is preserved. On the basis of these early studies Devincre and Condat (1992) and Devincre (1995) have pioneered the development of numerical 3D models in which dislocations are discretized in both space and time.

In the present investigation dislocations are described as static line defects which are embedded in an otherwise linear isotropic elastic medium. The dislocation lines are subdivided into small straight segments. For a given Burgers vector and glide plane normal, three different sorts of dislocation line segments emerge, namely screw type dislocations, glissile edge type dislocations, and jog type edge dislocations. The line segments involved represent translation vectors of the cubic lattice. For calculating the 3D stress field imposed by a dislocation, the linear elastic tensorial notation of Devincre (1995) is employed in the form:

$$\sigma_{ij}(\mathbf{r}) = A\left\{[\mathbf{bYt}]_{ij} - \frac{1}{1-\nu}\left([\mathbf{btY}]_{ij} + \frac{1}{2}(\mathbf{b}\cdot(\mathbf{Y}\times\mathbf{t})\left[\delta_{ij} + t_i t_j + \frac{2}{Y^2}\left(\rho_i Y_j + \rho_j Y_i + \frac{L}{|\mathbf{R}|}Y_i Y_j\right)\right]\right)\right\}, \tag{1}$$

with

$$A = \frac{G}{\pi Y^2}, \tag{2}$$

$$L = (\mathbf{R})\cdot\mathbf{t}, \tag{3}$$

$$\mathbf{Y} = (L + |\mathbf{R}|)\mathbf{t} + \boldsymbol{\rho}, \tag{4}$$

and the symmetrical tensor operators

$$[\mathbf{bYt}]_{ij} = \tfrac{1}{2}[(\mathbf{b} \times \mathbf{Y})_i t_j + (\mathbf{b} \times \mathbf{Y})_j t_i], \tag{5}$$

$$[\mathbf{btY}]_{ij} = \tfrac{1}{2}[(\mathbf{b} \times \mathbf{t})_i Y_j + (\mathbf{b} \times \mathbf{t})_j Y_i], \tag{6}$$

where **b** is the Burgers vector, **t** the unit tangent vector of the dislocation line segment, **R** the vectorial distance between the stress field coordinate and the central dislocation segment coordinate, **ρ** the portion of **R** which is normal to **t**, δ_{ij} the Kronecker symbol, G the shear modulus and ν Poisson's ratio. The portion of the stress field imposed by a single segment located between two coordinates A and B is computed according to

$$\sigma_{ij}^{AB}(\mathbf{r}) = [(\sigma_{ij}(\mathbf{r}))_{\mathbf{r}'=B} - (\sigma_{ij}(\mathbf{r}))_{\mathbf{r}'=A}]. \tag{7}$$

The stress tensor at each point under investigation is finally computed by linearly superimposing the elastic stresses of all dislocations which are positioned within a distance larger than the inner cut-off radius ($2b$) and smaller than the outer cut-off radius ($6667b$). Dislocations positioned within the inner cut-off circle are treated as having a distance $2b$. In the present study the stresses are given in units of $(Gb)/(2\pi d)$, and the spatial coordinates in units of $(2\pi d)$ where d is the average dislocation spacing. A value of 1/3 was used for Poisson's ratio ν throughout the study.

For both idealized dislocation arrangements under investigation, the internal stress fields are computed only in the cell (including its cell walls) which is embedded in the centre of a given 3D network. The cell in the centre of the network is hereafter referred to as the centre cell. The entire cell structure consists of n cells, where $n = 343$ ($7 \times 7 \times 7$ cells) for the subgrain structure and $n = 125$ ($5 \times 5 \times 5$ cells) for the interface structure. Owing to their long range stress fields all dislocations within a distance smaller than the outer cut-off radius are considered for the computation of the local stresses in the centre cell. Hence there are no artificial effects due to the absence or asymmetry of the neighbouring cell structure. For comparing the results of 3D and corresponding quasi 2D simulations (without screw segments) the components of the 3D stress tensors are calculated within a plane that intersects in the middle of the edge dislocation lines of a given ensemble (here the [001] crystal direction). For investigating the maximum shearing stresses the stress tensors are rotated parallel to their principal axes. This enables one to discuss the maximum predicted stresses without referring to a specific coordinate system. The crystal reference system ([100], [101], [001]) and the sample reference system (x, y, z) are not misorientated with respect to each other, i.e. [100] is parallel to x, [010] to y, and [001] to z.

§ 3. Investigated dislocation cell structures

3.1. *Dislocation cells as mesoscopical sources of internal stresses*

The present study concentrates on the contribution of screw type dislocation segments to internal stress fields of two types of idealized dislocation cell, namely pure subgrain structures and cell structures with interface dislocations. Both arrangements are regarded as microstructural units of many observed dislocation networks. Whilst the first type of cell is typical of microstructures resulting from

deformation at elevated homologous temperatures, the second is typical of microstructures arising from deformation at low homologous temperatures.

Most currently used micromechanical equations of state are based on three main conceptual ingredients. First, the dislocations are adequately regarded as the elementary carriers of internal stresses. Their quantitative contribution is directly expressed as the square root of their density. Second, the spatial distribution of the latter quantity is complementarily considered, for instance, by distinguishing regions of high and low dislocation densities. Third, in more elaborate approaches the 'quality' of stress in a micromechanical sense is included by considering the type and arrangements of the (net) dislocations. The latter information is required for clarifying whether one deals with screened, i.e. short range or with non-screened, i.e. long range stresses.

The first ingredient is typically included by using the Taylor equation ($t \sim \sqrt{\rho}$), the second by using the composite model (Mughrabi 1979) and the third by quantifying both the contribution and local arrangement of screw and edge dislocations, and of interface and non-interface dislocations. Especially the third aspect, namely the influence of the local dislocation arrangement, cannot easily be described by analytical approaches and hence justifies the employment of numerical techniques. Within this conventional framework it thus seems pertinent to speak not only of dislocations as elementary microstructural sources of internal stresses, but also of dislocation cells as elementary mesoscopical sources of internal stress. Whilst the view of a microstructural source of stress offers only one type of information, the latter approach comprises three sorts of independent information. Such a conceptual point of view justifies a closer look at the properties of the following types of idealized dislocation cell.

3.2. *Subgrain structure*

The first type of cell structure (Kuhlmann-Wilsdorf 1968, Bassim and Kuhlmann-Wilsdorf 1973, Kuhlmann-Wilsdorf and van der Merwe 1982) represents a low energy 3D chequerboard type pattern consisting of cubic cells. The cell size amounts to $D = 1000\,\text{nm}$. The cells have a common axis of misorientation, but an alternating sense of rotation from one cell to the next. In three dimensions each cell consists of two pairs of parallel small angle tilt boundaries and one pair of parallel twist boundaries with alternating sense of misorientation. Each tilt wall contributes 10 dislocations with a spacing of $d = 100\,\text{nm}$. Following Bassim and Kuhlmann-Wilsdorf (1973) the tilt walls should only lead to short range but the twist walls to long range stresses. However, the authors showed that the latter stress contribution should degrade due to the alternating sense of rotation of neighbouring cells. Subgrain structures of this type should thus be free of substantial long range stresses†.

†For the sake of completeness one must add that the predictions of Kuhlmann-Wilsdorf and co-workers were questioned by the observation of long range internal stresses in steady-state subgrain structures which were generated at high homologous temperatures (Borbély *et al.* 1993). In a recent study Sedlacek (1995) complemented this experimental result by also showing that in such low energy subgrain structures internal long range stresses can arise due to bowed out glide dislocations in the cell interiors. However, in the present study bowed out glide dislocations in the cell interiors of subgrains are not considered.

The present study focuses on the contribution of the twist boundaries to such low energy subgrain structures. For this purpose the cell structures under investigation are calculated both with and without twist boundaries. The latter case is hereafter referred to as the quasi 2D approach. The vectors which define the involved dislocations represent basic vectors of a simple cubic lattice. Figure 1 (*a*) shows an idealized quasi 2D dislocation arrangement containing only one type of tilt wall, i.e. only one slip system. Figure 1 (*b*) shows the completed ensemble containing both edge and screw dislocations. Figures 1 (*c*) and (*d*) show the corresponding idealized arrangements for the case of two involved slip systems. The latter example (fig. 1 (*d*)) exactly corresponds to the model of Kuhlmann-Wilsdorf and van der Merwe (1982).

3.3. *Cell structure consisting of interface dislocations*

Figure 2 shows the second type of investigated dislocation arrangement. It consists of thick cell walls with a high dislocation content and cell interiors which are void of dislocations (Mughrabi 1979). The diameter of the cell interior amounts to $D = 1000\,\text{nm}$. The cell walls have a thickness of $w = 100\,\text{nm}$. They typically consist of dislocation dipoles which are enriched by so-called interface dislocations (Mughrabi 1983). The dislocation dipoles in the cell walls do not lead to long range stresses and are neglected in the following. In the present simulation the interface dislocations have a spacing of $d = 100\,\text{nm}$. According to the original model of Mughrabi (1983) the involved dislocations have ⟨110⟩ Burgers vectors and ⟨110⟩ or ⟨100⟩ line vectors (fig. 2). The schematic sketch shows that the externally imposed stress is aligned parallel to the [010] direction. The direction of the external stress source is indicated by justifying the chosen dislocation arrangement. In the simulation the axis stress is equal to zero.

The interface dislocations represent geometrically necessary dislocations in the sense of Nye (1953), Cottrell (1964) and Ashby (1970). In microstructural terms interface dislocations are regarded as net dislocations resulting from the active slip systems in the cell interiors (Mughrabi 1983). Accounting for the fact that such dislocation substructures evolve during rather than subsequent to plastic deformation, Mughrabi (1979, 1983) studied the properties of dislocation cell structures in the stress-applied state under the constraint of strain compatibility of the cell walls and interiors. This requirement was shown to unavoidably lead to the formation of long range internal stress fields. For the description of compatibility a new class of dislocations, named interface dislocations, was introduced. In contrast to former studies in which long range stresses were attributed to dislocation pile-ups (Seeger, Diehl, Mader and Rebstock 1957), the approach of Mughrabi (1979, 1983) substantiated that long-range internal stresses are closely related to the requirement for compatibility in cell-containing structures in the stress-applied state.

In the first paper on this subject the contribution of screw type interface dislocations was neglected (Mughrabi 1983). However, in a short note which was added to an ensuing paper of Mughrabi *et al.* (1986) it is mentioned that analytical calculations suggested that the contribution of screw dislocations should considerably increase the internal long range stresses. However, except for this note and some qualitative comments, the stress fields associated with complex cell structures are until today typically calculated in two dimensions rather than three dimensions. This means regardless of Mughrabi *et al.*'s hint (1986), the influence of screw dislocations on internal stresses is usually entirely neglected.

Fig. 1

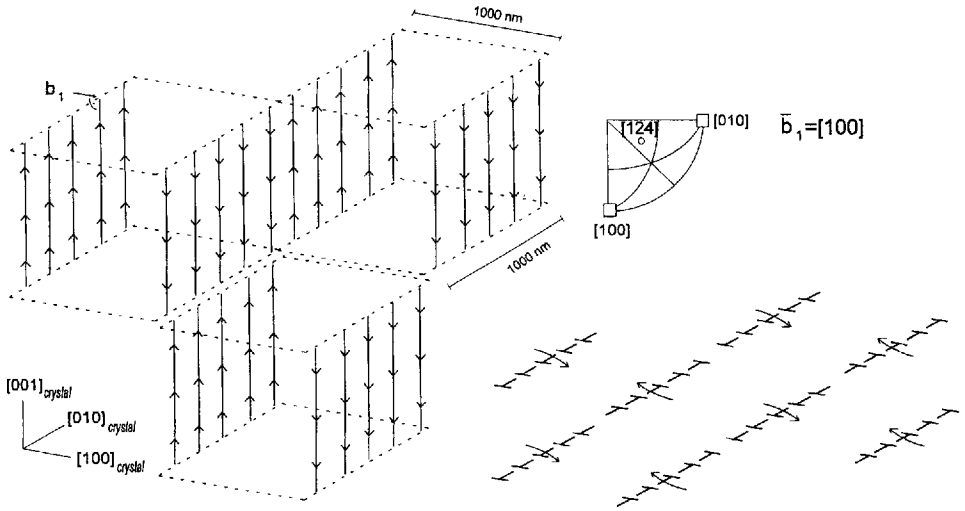
1000 nm
b1
1000 nm
[001]crystal
[010]crystal
[100]crystal
[124]
[010]
[100]
b̄1=[100]

(*a*)

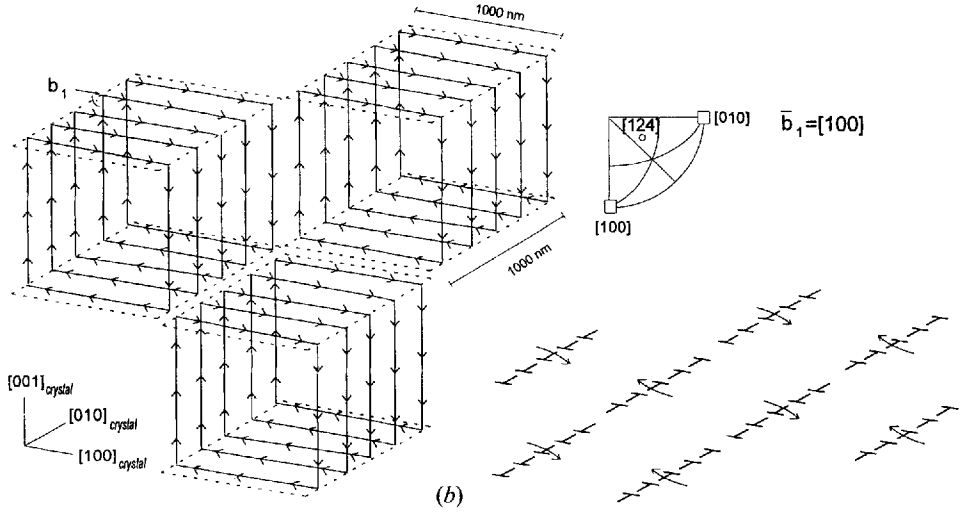
1000 nm
b1
1000 nm
[001]crystal
[010]crystal
[100]crystal
[124]
[010]
[100]
b̄1=[100]

(*b*)

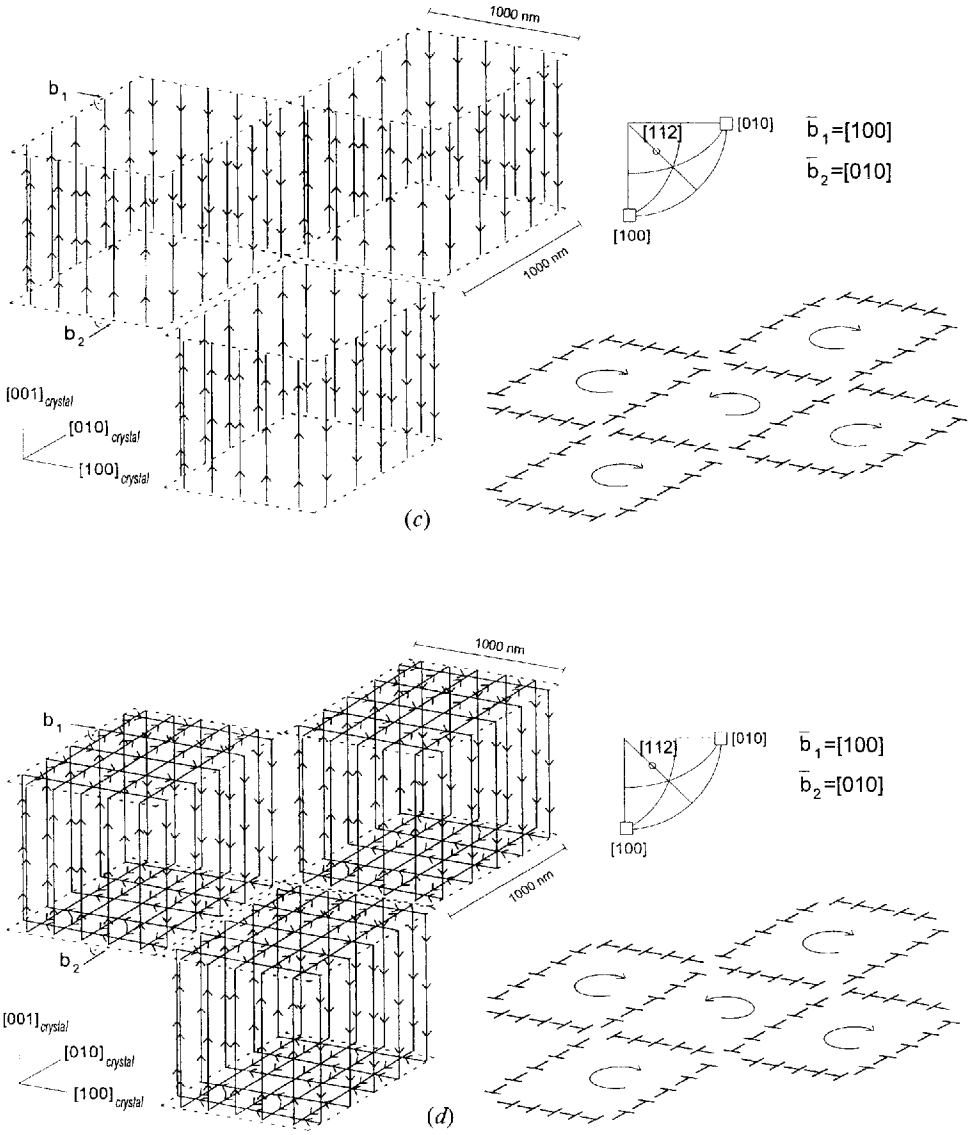

(*a*) Idealized quasi 2D dislocation arrangement containing only edge dislocations (single slip). Each tilt wall contributes 10 edge dislocations with a spacing of $d = 100$ nm. The cell diameter is $D = 1000$ nm. Screw dislocations are neglected. (*b*) Idealized 3D dislocation arrangement containing both edge and screw dislocations (single slip). Each wall contains 10 dislocations with a spacing of $d = 100$ nm. The cell diameter is $D = 1000$ nm. (*c*) Idealized quasi 2D dislocation arrangement containing only edge dislocations (double slip). Each tilt wall contributes 10 edge dislocations with a spacing of $d = 100$ nm. The cell diameter is $D = 1000$ nm. Screw dislocations are neglected. (*d*) Idealized 3D dislocation arrangement containing both edge- and screw dislocations (double slip). In the model each tilt wall contains 10 dislocations with a spacing of $d = 100$ nm. The twist walls contain 20 screw dislocations. The cell diameter is $D = 1000$ nm. This set-up corresponds to the model of Kuhlmann-Wilsdorf and van der Merwe (1982).

Fig. 2

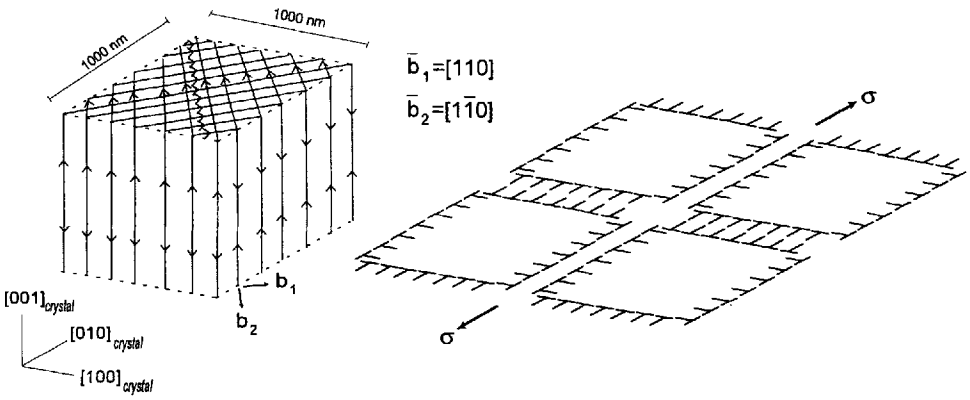

Idealized 3D dislocation arrangement consisting of thick cell walls with a high dislocation content and cell interiors which are void of dislocations (Mughrabi 1979). The cell diameter is $D = 1000$ nm. The cell walls have a thickness of 100 nm. The walls typically consist of dislocation dipoles which are enriched by interface dislocations (Mughrabi 1983). The dislocation dipoles in the cell walls do not lead to long range stresses and are hence neglected. In the present simulation the interface dislocations have a spacing of $d = 100$ nm. According to the original model of Mughrabi (1983) the involved dislocations have ⟨110⟩ Burgers vectors and ⟨110⟩ or ⟨100⟩ line vectors. The external stress is aligned parallel to the [010] direction. In the simulation the axis stress is equal to zero.

§ 4. Results and discussion

4.1. *Subgrain cell structure*

Figure 3 (*a*) shows the spatial distribution of the shear stress component, $\sigma(xy)$, in two neighbouring cells as a function of x and y at $z = D/2$ (D = cell diameter). The corresponding dislocation set-up is shown in fig. 1 (*a*). Since cell walls with equal sign succeed with a wavelength of two cell diameters (fig. 1 (*a*)), the stress distribution is shown for two adjacent centre cells. In this first ensemble the screw dislocations are ignored (fig. 1 (*a*)). The example may thus be regarded as a quasi 2D approach. Figure 3 (*a*) substantiates that in both cell interiors long range shear stresses occur. The array produces negative shear stresses in the first and positive stresses in the second cell. The stress peaks indicate the positions of the dislocations. Figure 4 (*a*) shows the corresponding profile of the maximum shearing stress at $y = D/4$ and $y = D/2$ (dotted lines) through the cell interior.

If the screw dislocation segments are additionally considered (fig. 1 (*b*)) a very similar shear stress distribution is predicted (figs 3 (*b*), 4 (*b*)). However, two relevant differences become apparent. First, the stress maximum associated with the latter configuration at $x/2(2\pi d) = 0{\cdot}8$ and $2{\cdot}4(y = D/2$ (fig. 4 (*b*)) exceeds that of the first one (fig. 4 (*a*)) by about 75%. Second, the shape of the shear stress distribution of the latter configuration (fig. 3 (*b*)) becomes more regular as compared to that of the incomplete ensemble (fig. 3(*a*)). This first simple example shows that the neglect of the screw dislocations can lead to an underestimation of internal long range stresses. Although the given example (fig. 1 (*a,b*)) reflects the importance of the screw

Fig. 3

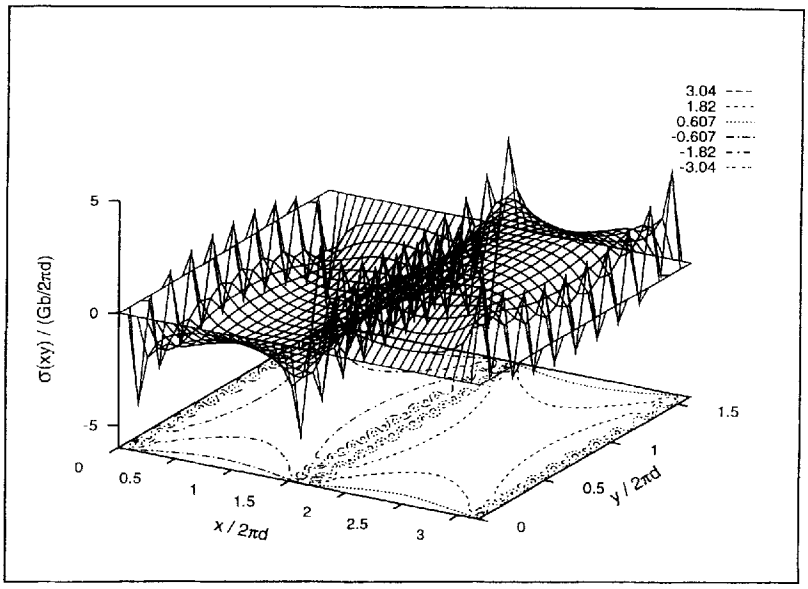
3.04
1.82
0.607
-0.607
-1.82
-3.04
σ(xy) / (Gb/2πd)
5
0
-5
0
0.5
1
1.5
2
2.5
3
x / 2πd
0
0.5
1
1.5
y / 2πd

(*a*)

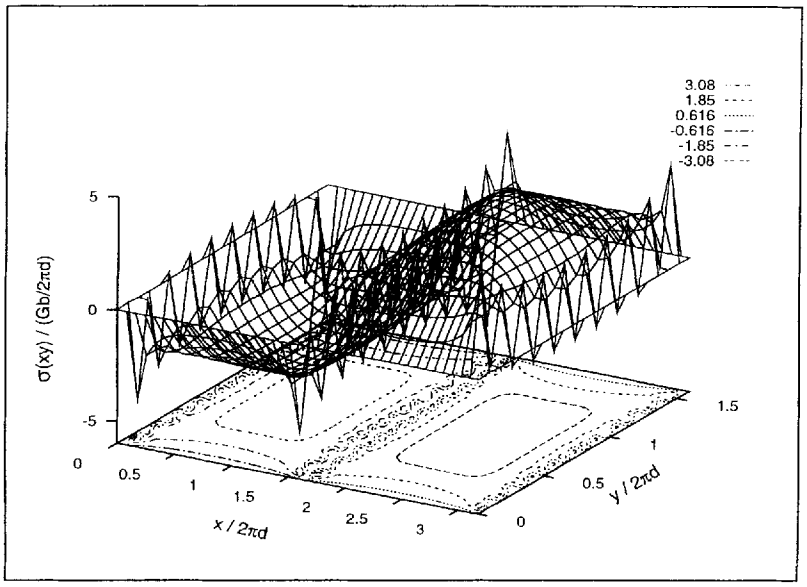
3.08
1.85
0.616
-0.616
-1.85
-3.08
σ(xy) / (Gb/2πd)
5
0
-5
0
0.5
1
1.5
2
2.5
3
x / 2πd
0
0.5
1
1.5
y / 2πd

(*b*)

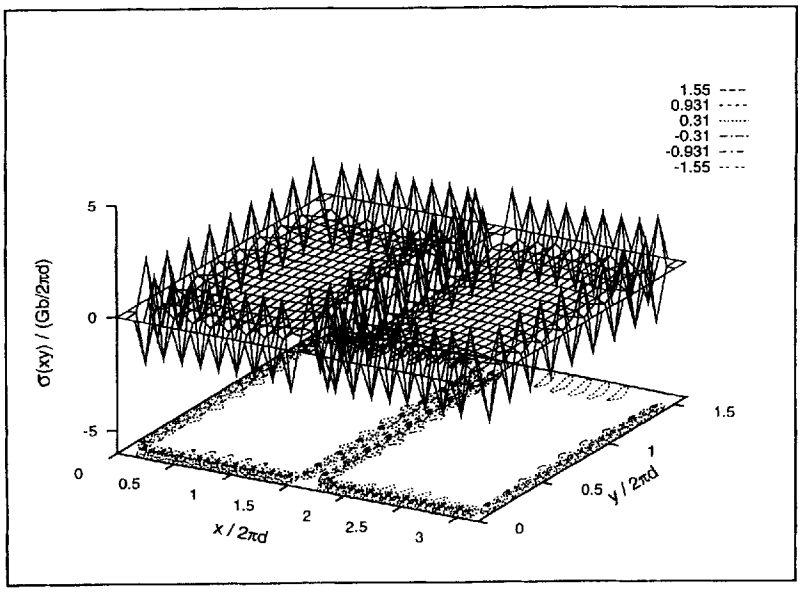

(*c*)

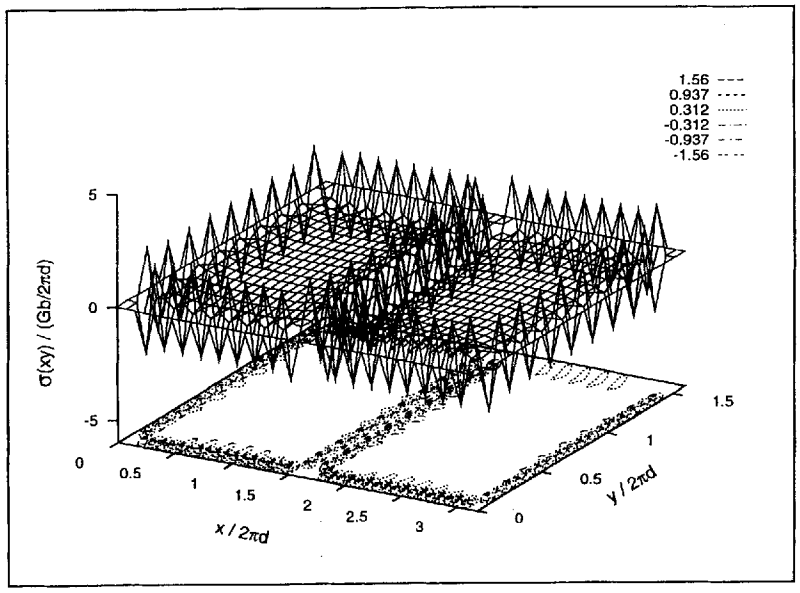

(*d*)

Spatial distribution of the shear stress component, $\sigma(xy)$, in two neighbouring cells as a function of x and y at $z = D/2$ (D = cell diameter). The stresses are given in units of $(Gb)/(2\pi d)$, and the spatial coordinates in units of $(2\pi d)$ (d = dislocation spacing). Since cell walls with equal sign succeed with a wavelength of two cell diameters, the stress distribution is shown for two adjacent cells. (*a*) Shear stress distribution for the dislocation arrangement shown in fig. 1 (*a*). (*b*) Shear stress distribution for the dislocation arrangement shown in fig. 1 (*b*). (*c*) Shear stress distribution for the dislocation arrangement shown in fig. 1 (*c*). (*d*) Shear stress distribution for the dislocation arrangement shown in fig. 1 (*d*).

Fig. 4

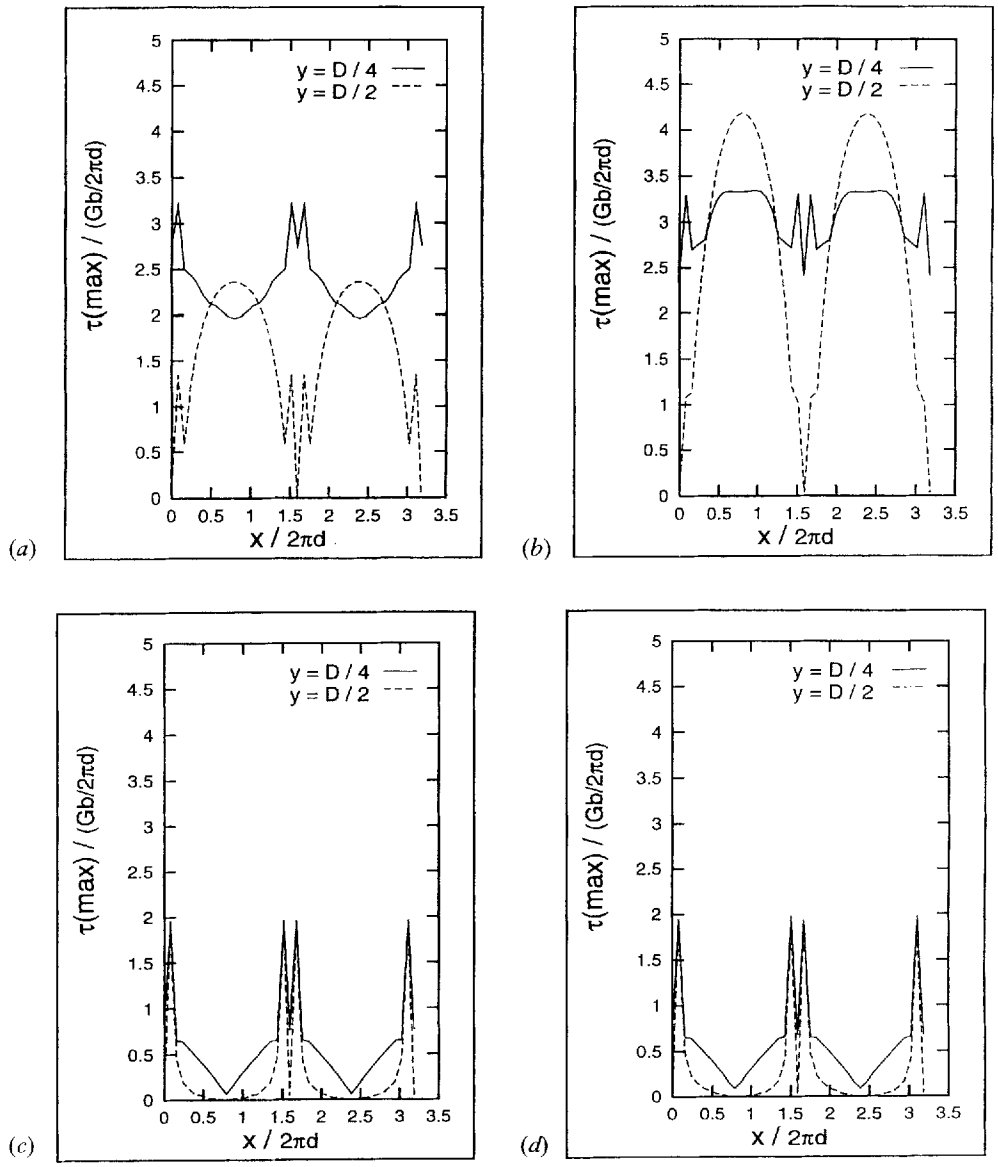

Profile of the maximum shearing stress, $\tau(\max)$, at $y = D/4$ and $y = D/2$ through the cell interior of two neighbouring cells (D = cell diameter). The stresses are given in units of $(Gb)/(2\pi d)$, and the spatial coordinates in units of $(2\pi d)$ (d = dislocation spacing). (*a*) Shear stress distribution for the dislocation arrangement shown in fig. 1 (*a*); edge and screw dislocations are considered, quasi 2D approach (single slip). (*b*) Shear stress distribution for the dislocation arrangement shown in fig. 1 (*b*); only edge and screw dislocations are considered, 3D approach (single slip). (*c*) Shear stress distribution for the dislocation arrangement shown in fig. 1 (*c*); only edge dislocations are considered, quasi 2D approach (double slip). (*d*) Shear stress distribution for the dislocation arrangement shown in fig. 1 (*d*); edge and screw dislocations are considered, 3D approach (double slip).

dislocations, the evolution of cell structures with only one slip system being active is not very realistic.

Thus, in the following the stress distribution associated with an idealized subgrain cell structure involving two types of perpendicular slip system is considered. This model corresponds to the set-up outlined in the paper of Kuhlmann-Wilsdorf and van der Merwe (1982). Again, the calculations are carried out both with and without twist boundaries (fig. 1 (*c,d*)). Figures 3 (*c,d*) and 4 (*c,d*) show that no long range stresses occur in the cell interiors irrespective of the contribution of twist boundaries. This result justifies that, if no long range stresses occur, one may indeed reduce stress field calculations of subgrain structures from three dimensions to two dimensions. However, according to footnote 1, this statement is confined to ensembles where the presence of bowed out glide dislocations in the cell interiors of subgrains is excluded.

4.2. *Cell structure with interface dislocations*

Figures 5 and 6 show the spatial distribution of the normal stresses, $\sigma(xx)$ and $\sigma(yy)$, in the centre cell of a translational ensemble consisting of interface dislocations. Figure 2 shows that the tensile stress is applied parallel to the crystal [010] axis. Whilst figs 5 (*a*) and 6 (*a*) show the stress fields in the quasi 2D approach, i.e. without twist boundaries, figs 5 (*b*) and 6 (*b*) show the stress components as determined for the complete arrangement (fig. 2). Except for quantitative differences both arrangements lead to similar shapes of their internal long range stress fields. The stress distribution in the cell interior is in both cases characterized by a tensile stress perpendicular and by a compressive stress parallel to the external tensile stress axis. The externally applied stress is equal to zero. The calculated stress distribution is in very good accord with the predictions of Mughrabi (1983), and Mughrabi *et al.* (1986). Figures 7, 8 and 9 show three profiles of two normal stress components and of the maximum shearing stress through the centre cell. The three curves depicted in each diagram represent the stress at $y = D$, $y = D/2$ (solid lines), and $y = D/4$. While figs 7 (*a*), 8 (*a*) and 9 (*a*) show the stress fields in ensembles without twist boundaries, figs 7 (*b*), 8 (*b*) and 9 (*b*) show the stresses associated with the complete dislocation arrangement (fig. 2). In the latter case a considerable increase in the internal tensile stress, $\sigma(xx)$, and a decrease in internal compressive stress, $\sigma(yy)$, is observed as compared to the corresponding stress components associated with the incomplete cell. Accordingly, the maximum shearing stress is much larger in the complete cell which contains both edge and screw dislocations (fig. 9 (*b*)) than in the quasi 2D approach where the latter dislocations are neglected (fig. 9 (*a*)). Due to the influence of the twist walls, the maximum shearing stress in the cell interior rises by 67%.

This increase can qualitatively be described by a simple empirical equation. Denoting the shearing stress in the quasi 2D cell which considers only edge dislocations as τ^{2D} (fig. 9 (*a*)) and the additional contribution arising from the screw dislocations as $\tau^{2D}(1 - \nu)$, the total shearing stress level in the 3D ensemble, τ^{3D} (fig. 9 (*b*)), can be empirically described by expression (8). In this equation ν represents Poisson's ratio, which in all calculations had a value of 1/3.

$$\tau^{3D} = \tau^{2D} + \tau^{2D}(1 - \nu) = \tau^{2D}(2 - \nu). \tag{8}$$

This qualitative description is in reasonable accord with the analytical study of Mughrabi *et al.* (1986). In a note added in proof, Mughrabi *et al.* (1986) mentioned

Fig. 5

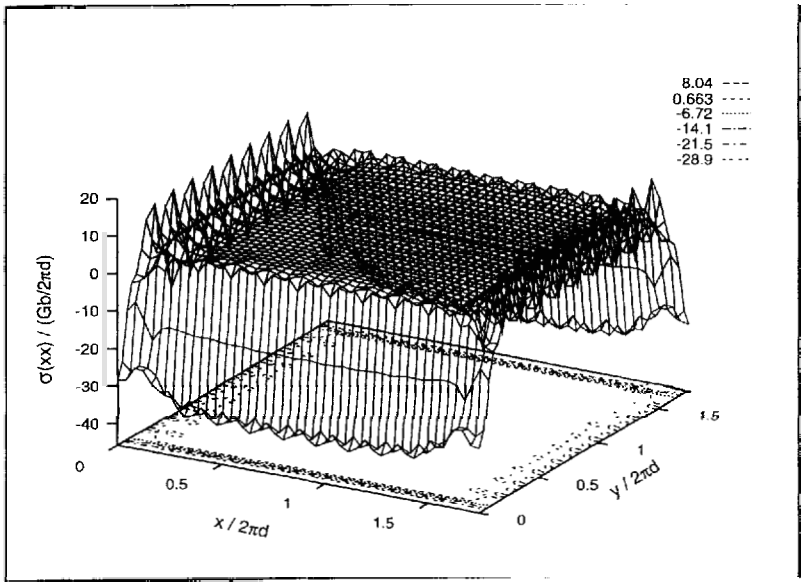

(*a*)

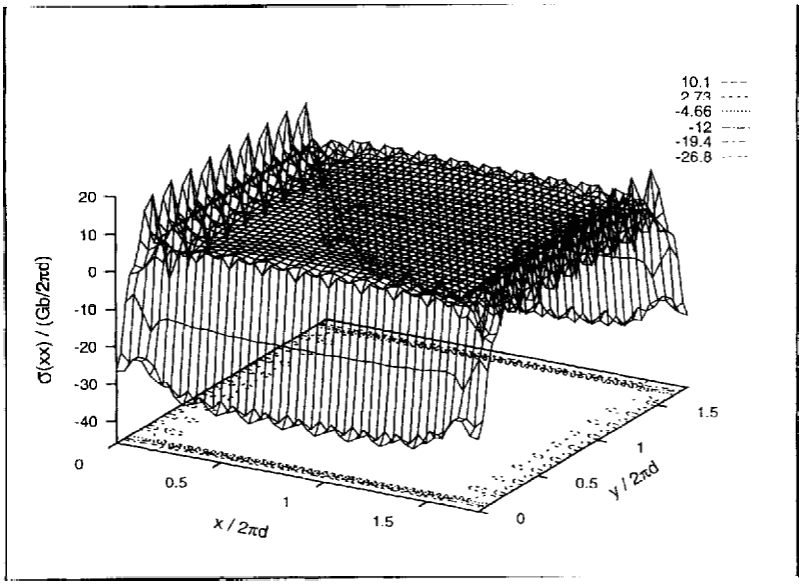

(*b*)

Spatia distribution of the normal stress component, $\sigma(xx)$, for the configuration shown in fig. 2 as a function of x and y at $z = D/2$ (D = cell diameter). The stress component $\sigma(xx)$ is perpendicular to the external stress axis. The stresses are given in units of $(Gb)/(2\pi d)$, and the spatial coordinates in units of $(2\pi d)$ (d = dislocation spacing). (*a*) $\sigma(xx)$, normal stress component perpendicular to the external stress axis; only edge dislocations are considered, quasi 2D approach. (*b*) $\sigma(xx)$, normal stress component perpendicular to the external stress axis; edge and screw dislocations are considered, 3D approach.

Fig. 6

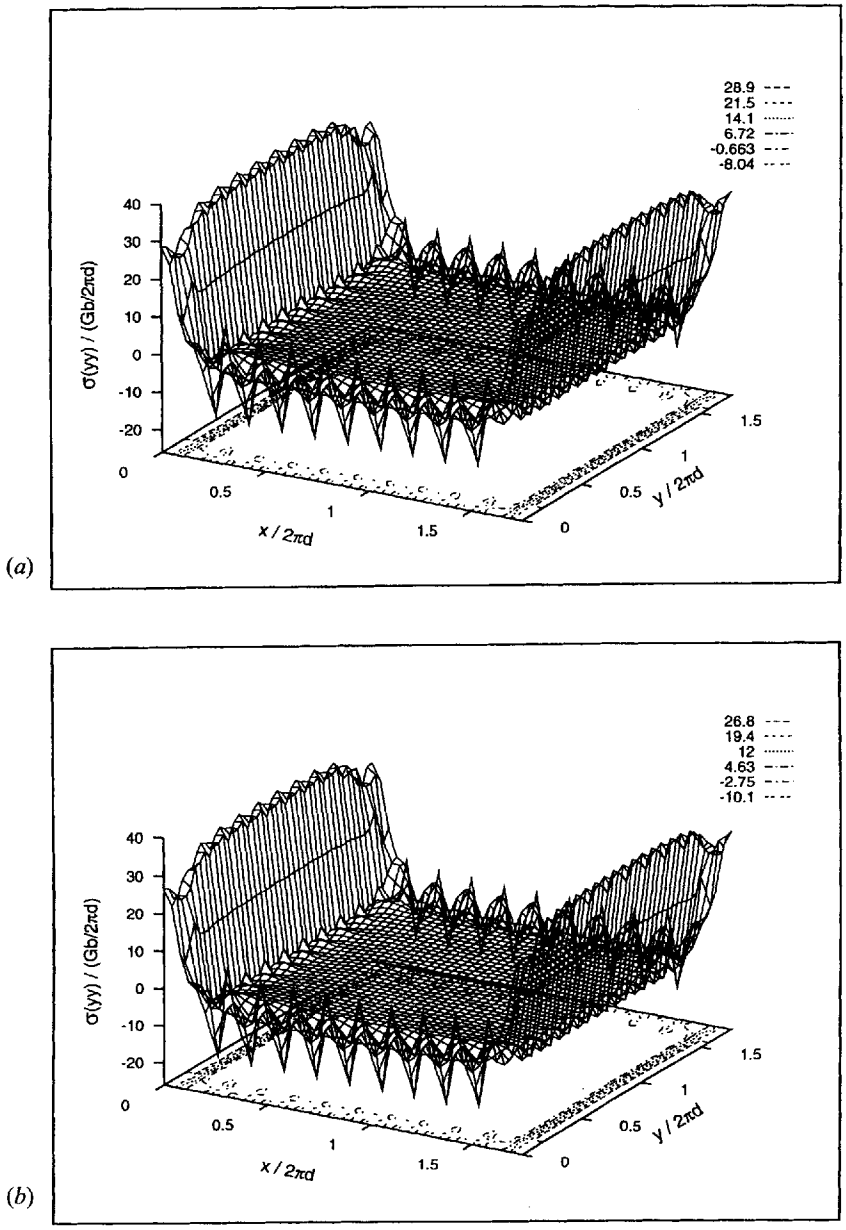

Spatial distribution of the normal stress component, $\sigma(yy)$, for the configuration shown in fig. 2 as a function of x and y at $z = D/2$ (d = cell diameter). The stress component $\sigma(yy)$ is parallel to the external stress axis. The stresses are given in units of $(Gb)/(2\pi d)$, and the spatial coordinates in units of $(2\pi d)$ (d = dislocation spacing). (*a*) $\sigma(yy)$, normal stress component parallel to the external stress axis; only edge dislocations are considered, quasi 2D approach. (*b*) $\sigma(yy)$, normal stress component parallel to the external stress axis; edge and screw dislocations are considered, 3D approach.

Fig. 9

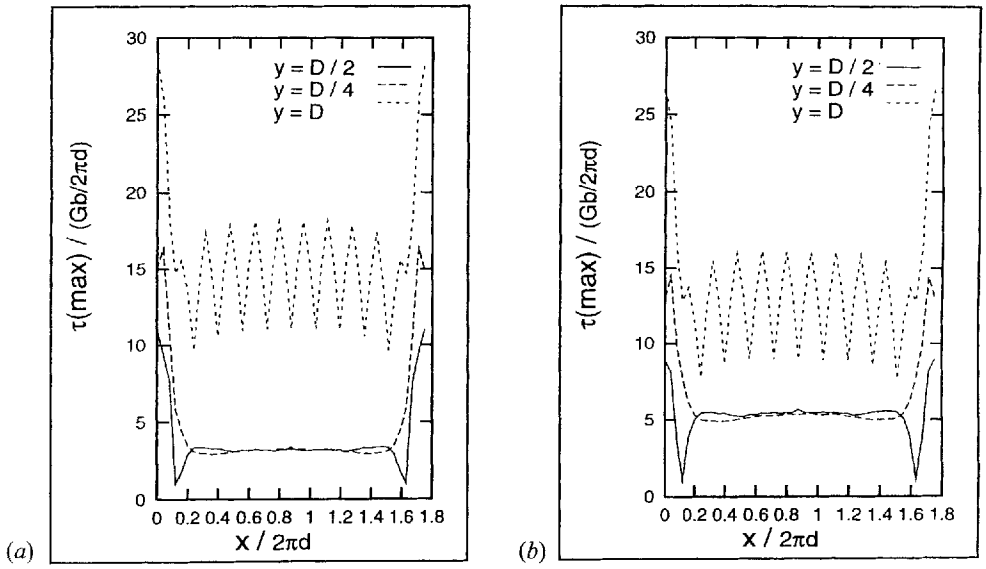

Profile of the maximum shearing stress, $\tau(\max)$, at $y = D/2$, $y = D/4$ and $y = D$ through the cell interior for the configuration shown in fig. 2 (D = cell diameter). The stresses are given in units of $(Gb)/(2\pi d)$, and the spatial coordinates in units of $(2\pi d)$ (d = dislocation spacing). (*a*) $\tau(\max)$, maximum shearing stress; only edge dislocations are considered, quasi 2D approach. (*b*) $\tau(\max)$, maximum shearing stress; edge and screw dislocations are considered, 3D approach.

4.3. *Structural simplifications in dislocation models*

One of the most important tasks in the field of simulation is the rendering of structural symmetries inherent to real mesoscopical dislocation arrangements into models for achieving conceptual simplification. In this context various rearrangements of the dislocations involved in the discussed ensembles were investigated. The underlying principle of all simplifications is schematically sketched in fig. 11. After decomposing the dislocations in the interface structure (fig. 2) into small portions, some elements undergo annihilation (elements 'd' and 'D' in fig. 11 (*a*)) whilst others recombine (elements 'e' and 'C' or 'E' and 'c'). If spatial aspects are neglected, such a procedure can lead to a rearrangement as sketched in fig. 11 (*b*). However, the present study revealed that such simplification can lead to considerable mispredictions of the resulting stress fields. This is especially true for cell structures that generate long range stresses. In such cases the spatial distribution of the segments arising from decomposed dislocations is of great importance. The numerical errors

Fig. 8

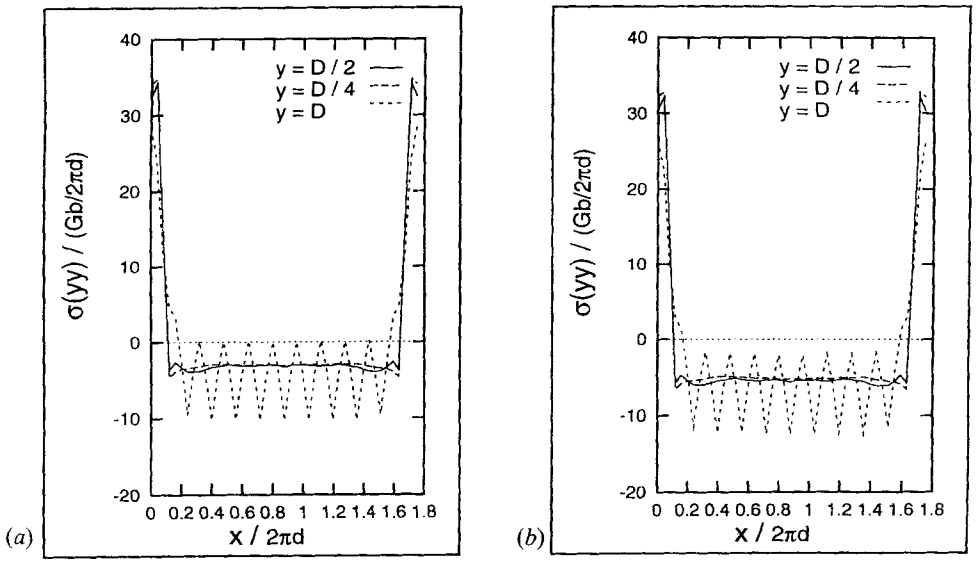

Profile of the normal stress component, $\sigma(yy)$, at $y = D/2$, $y = D/4$ and $y = D$ through the cell interior for the configuration shown in fig. 2 (D = cell diameter). The stresses are given in units of $(Gb)/(2\pi d)$, and the spatial coordinates in units of $(2\pi d)$ (d = dislocation spacing). (*a*) $\sigma(yy)$, normal stress component perpendicular to the external stress axis; only edge dislocations are considered, quasi 2D approach. (*b*) $\sigma(yy)$, normal stress component perpendicular to the external stress axis; edge and screw dislocations are considered, 3D approach.

The stress contribution of the two additional slip systems can then be derived by

$$\boldsymbol{\sigma}^{90^\circ} = (\mathbf{g}^{90^\circ}_{[010]})^{-1}\boldsymbol{\sigma}\mathbf{g}^{90^\circ}_{[010]}, \tag{10}$$

where $\boldsymbol{\sigma}$ is the original stress tensor as partially depicted in figs 5–9, $\boldsymbol{\sigma}^{90^\circ}$ the rotated stress tensor which expresses the contribution of the two additional slip systems, and $(\mathbf{g}^{90^\circ}_{[010]})^{-1}$ the inverse rotation matrix. Since the latter matrix is derived for orthogonal and normalised lattice vectors, its transposed form corresponds to its inverse form, i.e. $(\mathbf{g}^{90^\circ}_{[010]})^{-1} = (\mathbf{g}^{90^\circ}_{[010]})^{\mathrm{T}}$. The total internal stress field, $\boldsymbol{\sigma}^{\mathrm{total}}$, of a cell with four different slip systems can thus be computed from the original stress field according to

$$\boldsymbol{\sigma}^{\mathrm{total}} = \boldsymbol{\sigma} + \boldsymbol{\sigma}^{90^\circ} = \boldsymbol{\sigma} + (\mathbf{g}^{90^\circ}_{[010]})^{\mathrm{T}}\boldsymbol{\sigma}\mathbf{g}^{90^\circ}_{[010]} = \begin{pmatrix} (\sigma_{xx}+\sigma_{zz}) & (\sigma_{xy}+\sigma_{yz}) & 0 \\ (\sigma_{xy}+\sigma_{yz}) & 2\sigma_{yy} & (\sigma_{yz}-\sigma_{xy}) \\ 0 & (\sigma_{yz}-\sigma_{xy}) & (\sigma_{xx}+\sigma_{zz}) \end{pmatrix}. \tag{11}$$

Figure 10 shows the normal stress component $\sigma(zz)$, as derived for the ensemble with two slip systems (fig. 2). It does not contribute any long range stresses. Equation (11) shows that due to the additional slip systems, the compression stress component parallel to [010], $\sigma(yy)$, is doubled whilst that perpendicular to [010], $\sigma(xx) + \sigma(zz)$, is now symmetrical with respect to the tensile axis.

Fig. 9

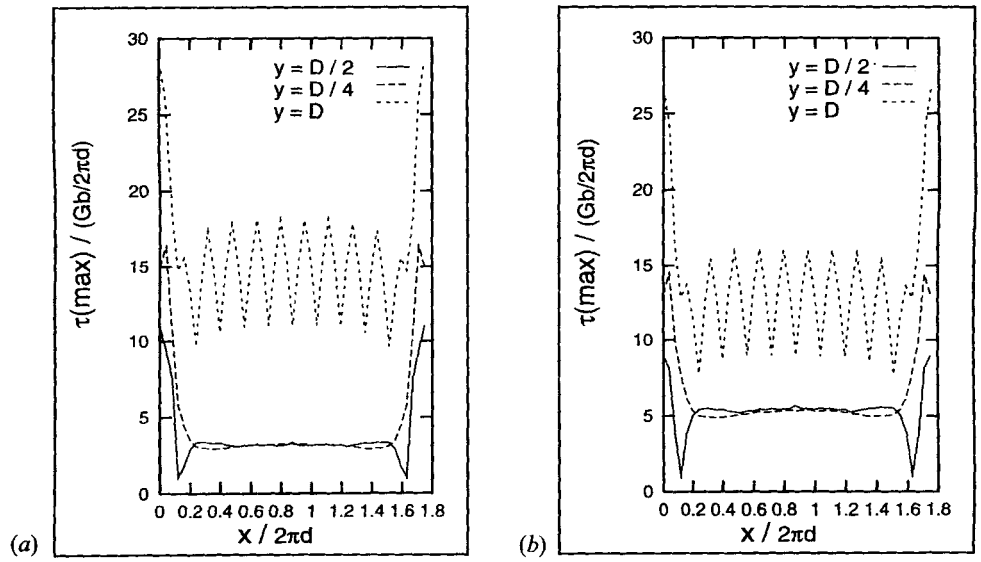

Profile of the maximum shearing stress, $\tau(\max)$, at $y = D/2$, $y = D/4$ and $y = D$ through the cell interior for the configuration shown in fig. 2 (D = cell diameter). The stresses are given in units of $(Gb)/(2\pi d)$, and the spatial coordinates in units of $(2\pi d)$ (d = dislocation spacing). (*a*) $\tau(\max)$, maximum shearing stress; only edge dislocations are considered, quasi 2D approach. (*b*) $\tau(\max)$, maximum shearing stress; edge and screw dislocations are considered, 3D approach.

4.3. *Structural simplifications in dislocation models*

One of the most important tasks in the field of simulation is the rendering of structural symmetries inherent to real mesoscopical dislocation arrangements into models for achieving conceptual simplification. In this context various rearrangements of the dislocations involved in the discussed ensembles were investigated. The underlying principle of all simplifications is schematically sketched in fig. 11. After decomposing the dislocations in the interface structure (fig. 2) into small portions, some elements undergo annihilation (elements 'd' and 'D' in fig. 11 (*a*)) whilst others recombine (elements 'e' and 'C' or 'E' and 'c'). If spatial aspects are neglected, such a procedure can lead to a rearrangement as sketched in fig. 11 (*b*). However, the present study revealed that such simplification can lead to considerable mispredictions of the resulting stress fields. This is especially true for cell structures that generate long range stresses. In such cases the spatial distribution of the segments arising from decomposed dislocations is of great importance. The numerical errors stemming from such geometrical simplifications increase with the ratio of the dislocation spacing to the segment length, L_1/L_2 (fig. 11). Therefore simplifications should only be employed when the occurrence of long range stresses can be excluded. Self screening microstructural elements such as dislocation dipoles can generally be ignored in discussing long range stress fields. These statements are only valid for static problems. In the case of dynamic aspects they do not generally apply.

Fig. 10

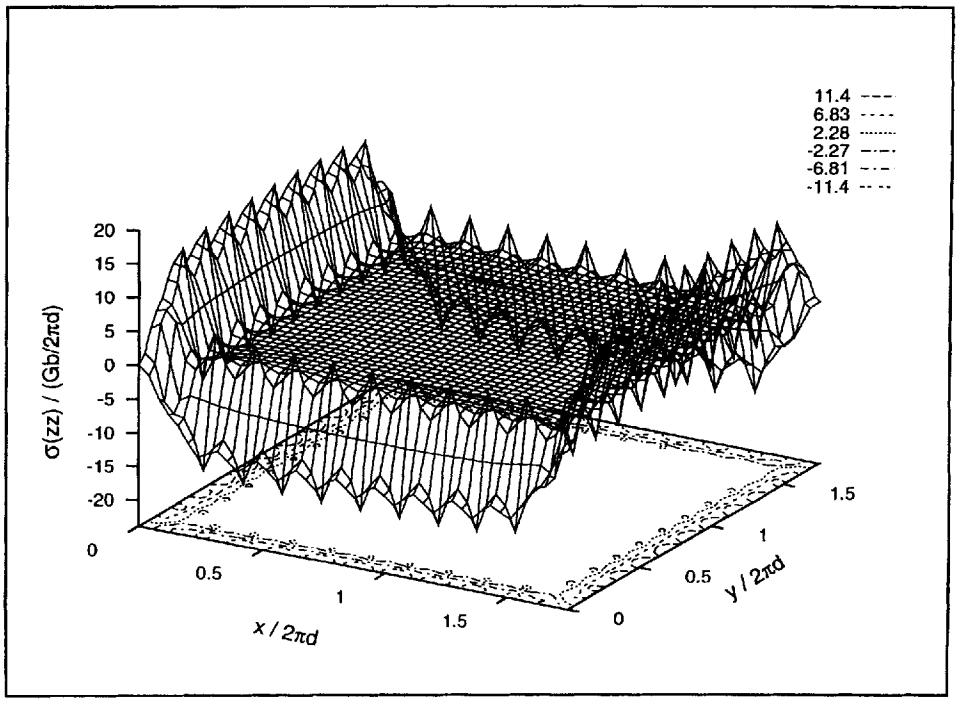

Spatial distribution of the normal stress component $\sigma(zz)$ for the configuration shown in fig. 2 as a function of x and y at $z = D/2$ (D = cell diameter). The stresses are given in units of $(Gb)/(2\pi d)$, and the spatial coordinates in units of $(2\pi d)$ (d = dislocation spacing). Edge and screw dislocations are considered, 3D approach.

4.4. *Boundary conditions*

Dislocations can principally impose long range stresses. For this reason the boundary conditions of a simulation considerably influence the numerical results. Figure 12 shows the maximum shearing stress as determined for the interface cell structure without considering the neighbouring cells. When comparing these results with the predictions depicted in fig. 9, two main deviations emerge. First, the maximum occurring value of stress in the cell interior increases and second, the shape of the stress field is less homogeneous when the neighbouring cells are neglected (fig. 12). Whilst in the case of adequate boundary conditions (fig. 9) the course of the stress is nearly horizontal, in the case of inadequate boundary conditions (fig. 12) a stress minimum occurs in the cell interior. The deviations appear both if the stress fields are calculated with (fig. 12 (*b*)) and without screw dislocations (fig. 12 (*a*)).

§ 5. Conclusions

The stress fields arising from subgrain and interface type dislocation ensembles were investigated using 3D simulations. The stress fields were calculated for cells with and without screw dislocations. The first type of calculation represented a 3D and the latter a quasi 2D approach. The main conclusions are:

Fig. 11

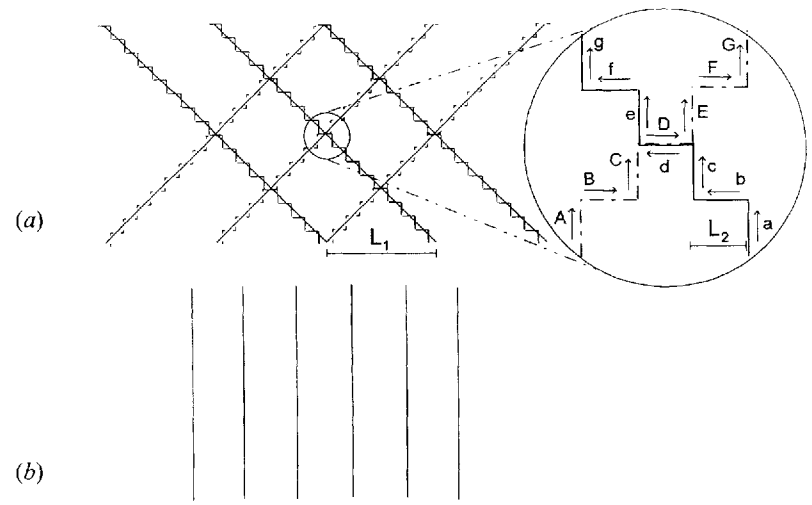

Principle of structural simplifications. After decomposing the dislocations in the interface structure (fig. 2) into small portions, some elements undergo annihilation (elements 'd' and 'D') whilst others recombine (elements 'e' and 'C' or 'E' and 'c'). If spatial aspects are neglected such a procedure can lead to a rearrangement as sketched in fig. 11 (*b*). However, the present study showed that such simplification can lead to considerable errors.

Fig. 12

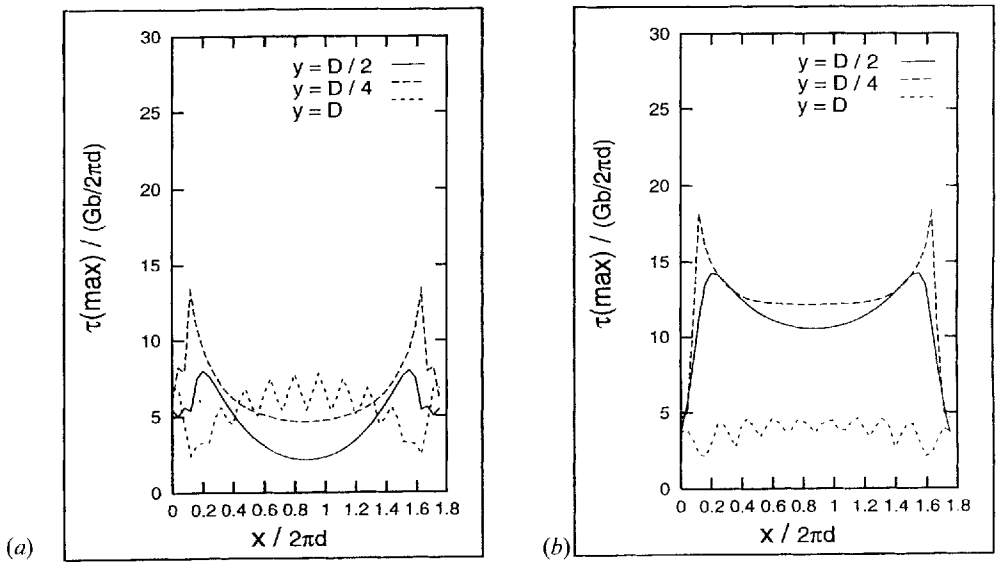

Profile of the maximum shearing stress, $\tau(\max)$, at $y = D/2$, $y = D/4$ and $y = D$ through the cell interior for the interface cell structure shown in fig. 2 (D = cell diameter). In contrast to the stress profiles shown in fig. 9, in this example, the maximum shearing stress was determined without considering the neighbouring cells. The stresses are given in units of $(Gb)/(2\pi d)$, and the spatial coordinates in units of $(2\pi d)$ (d = dislocation spacing). (*a*) $\tau(\max)$, maximum shearing stress; only edge dislocations are considered, quasi 2D approach. (*b*) $\tau(\max)$, maximum shearing stress; edge and screw dislocations are considered, 3D approach

(1) In subgrain structures the contribution of screw dislocations to internal stresses is negligible. This statement is valid only for the case that no bowed out glide dislocations occur in the cell interiors. The results obtained for subgrain structures can be extended to any case where no long range stresses occur. A correction of stresses predicted from 2D analytical and 2D numerical models is not required.

(2) In cell structures containing dislocations, the contribution of screw dislocations to internal stresses is not negligible. In the present example the screw dislocations led to an increase in the maximum shearing stress in the cell interior by about 67%. The total value of the maximum shearing stress arising from screw and edge dislocations, τ^{3D}, was empirically described by the expression $\tau^{3D} = \tau^{2D} + \tau^{2D}(1 - \nu)$, where τ^{2D} is the contribution of the edge and $\tau^{2D}(1 - \nu)$ that of the screw dislocations.

ACKNOWLEDGMENTS

The author gratefully acknowledges helpful discussions with Professor W. Blum and Professor H. Mughrabi.

REFERENCES

ASHBY, M. F., 1970, *Phil. Mag.*, **21**, 399.

BASSIM, M. N., and KUHLMANN-WILSDORF, D., 1973, *Phys. Stat. sol.* A, **16**, 241; 1973, *Ibid.*, **17**, 281; 1973, *Ibid.*, **17**, 379.

BORBÉLY, A., MAIER, H. J., RENNER, H., STRAUB, S., UNGÁR, T., and BLUM, W., 1993, *Scripta metall.*, **29**, 7.

COTTRELL, A. H., 1964, *The Mechanical Properties of Matter* (New York: Wiley), p. 277.

DEVINCRE, B., 1995, *Solid St. Commun.*, **39**, 875.

DEVINCRE, B., and CONDAT, M., 1992, *Acta metall.*, **40**, 2629.

DEWIT, R., 1965, *Acta metall.*, **13**, 1210; 1967, *Phys. Stat. sol.*, **20**, 567, 575.

HOKANSON, J. L., 1963, *J. appl. Phys.*, **34**, 2337.

KUBIN, L. P., 1993, *Materials Science and Technology*, Vol. 6, edited by R. W. Cahn, P. Haasen and E. J. Kramer, volume editor H. Mughrabi (Weinheim: VCH), p. 137.

KUBIN, L. P., CANOVA, G. R., CONDAT, M., DEVINCRE, B., PONTIKIS, V., and BRECHET, Y., 1992, *Solid St. Phenom.*, **23,24**, 455.

KUHLMANN-WILSDORF, D., 1968, *Workhardening*, edited by J. Hirth and J. Weertmann (New York: Gordon and Breach), p. 97.

KUHLMANN-WILSDORF, D., and van der MERWE, J. H., 1982, *Mater. Sci. Engng*, **55**, 79.

LI, J. C. M., 1965, Acta metall., **13**, 931.

MUGHRABI, H., 1979, *Proceedings of the 5th International Conference on the Strength of Metals and Alloys*, Aachen, Germany, 27–31 August, Vol. 3, edited by P. Haasen, V. Gerold and G. Kostorz (Oxford: Pergamon Press); 1983, *Acta metall.*, **31**, 1367.

MUGHRABI, H., UNGÁR, T., KIENLE, W., and WILKENS, M., 1986, *Phil. Mag.*, **53**, 793.

NYE, J. F., 1953, *Acta metall.*, **1**, 153.

SEDLACEK, R., 1995, *Scripta metall.*, **33**, 283.

SEEGER, A., DIEHL, J., MADER, S., and REBSTOCK, H., 1957, *Phil. Mag.*, **2**, 323.

YOFFE, E. H., 1960, *Phil. Mag.*, **5**, 161.